Received: 19 September 2017 | Revised: 21 November 2017 | Accepted: 28 November 2017

DOI: 10.1002/bio.3447

RESEARCH ARTICLE

WILEY LUMINESCENCE
The Journal of Biological and Chemical Luminescence

Luminescent thermometer based on Eu^{3+}/Tb^{3+}-organic-functionalized mesoporous silica

Anna M. Kaczmarek[1] | Dolores Esquivel[2] | Brecht Laforce[3] | Laszlo Vincze[3] | Pascal Van Der Voort[4] | Francisco J. Romero-Salguero[2] | Rik Van Deun[1]

[1] L^3 – Luminescent Lanthanide Lab, Department of Chemistry, Ghent University, Ghent, Belgium

[2] Departamento de Quimica Organica, Instituto Universitario de Investigacion en Quimica Fina y Nanoquimica IUIQFN, Facultad de Ciencias, Universidad de Córdoba, Córdoba, Spain

[3] XMI group, Department of Chemistry, Ghent University, Ghent, Belgium

[4] COMOC, Department of Chemistry, Ghent University, Ghent, Belgium

Correspondence
Anna M. Kaczmarek and Rik Van Deun, L^3 – Luminescent Lanthanide Lab, Department of Chemistry, Ghent University, B-9000 Ghent, Belgium.
Email: anna.kaczmarek@ugent.be; rik.vandeun@ugent.be

Funding information
Spanish Ministry of Economy and Competitiveness, Grant/Award Number: MAT2013-44463-R; Bijzonder Onderzoeksfonds, Ghent University, Grant/Award Number: BOF15/PDO/091

Abstract

In this work we investigate a mesoporous silica (MS) decorated with dipyridyl-pyridazine (dppz) ligands and further grafted with a mixture of Eu^{3+}/Tb^{3+} ions (28.45%:71.55%), which was investigated as a potential thermometer in the 10–360 K temperature range. The MS material was prepared employing a hetero Diels–Alder reaction: 3,6-di(2-pyridyl)-1,2,4,5-tetrazine was reacted with the double bonds of vinyl-silica (vSilica) followed by an oxidation procedure. We explore using the dppz-vSilica material to obtain visible emitting luminescent materials and for obtaining a luminescent thermometer when grafted with Eu^{3+}/Tb^{3+} ions. For the dppz-vSilica@Eu,Tb material absolute sensitivity S_a of 0.011 K^{-1} (210 K) and relative sensitivity S_r of 1.32 $\%K^{-1}$ (260 K) were calculated showing good sensing capability of the material. Upon temperature change from 10 K to 360 K the emission color of the material changed gradually from yellow to red.

KEYWORDS

organic-functionalized silica, ratiometric sensors, temperature sensors

1 | INTRODUCTION

Organic-functionalized mesoporous silica (MS), as well as periodic mesoporous organosilica (PMO), grafted with lanthanide (Ln^{3+}) ions or complexes are an interesting class of hybrid organic–inorganic materials, which have been investigated for their use in luminescence applications.[1–6] These materials are promising 'platforms' for binding Ln^{3+} ions and Ln^{3+} complexes due to their large surface areas, well-ordered nanoporous structures and the possibility to incorporate organic groups, which can be further functionalized. This allows the formation of hybrid Ln^{3+} materials, which can show a wide range of luminescence properties both in the visible and near-infrared (NIR) region.[7,8]

It is well known that Ln^{3+} ions have very interesting luminescence properties. These properties are primarily due to the well-shielded nature of the 4f-4f transitions.[9,10] Ln^{3+} ions exhibit narrow emission peaks from the ultraviolet-visible (UV-vis) to NIR region, and they have significantly long decay times as well as high quantum yields. A significant downside of Ln^{3+} ions is that they have very low absorption coefficients. This is due to the 4f-4f transitions being parity forbidden by the Laporte rule. As a way to tackle this problem many hybrid (organic–inorganic) materials have been developed, which enable exciting the Ln^{3+} ion using the organic ligand (the so called 'antenna effect').[11,12]

MS materials, for example SBA-15, SBA-16, MCM-41 and MCM-48 have already been combined with various organic ligands, for example modified β-diketonates, pyridyl groups, 1,10-phenathroline and calix[4]arene derivatives. Some of these materials have further been explored as 'platforms' for covalent grafting of Ln^{3+} ions/complexes. For example MS nanospheres grafted with Ln^{3+} complexes (Ln = Eu^{3+}, Tb^{3+}, Sm^{3+}, Nd^{3+}, Yb^{3+}) using 2-(5-bromothiophen)

Abbreviations used: BET, Brunauer–Emmett–Teller; dppz, dipyridyl-pyridazine; Ln^{3+}, lanthanide ion; MS, mesoporous silica; MOF, metal organic framework; PMO, periodic mesoporous organosilica; PXRD, powder X-ray diffraction; S_a, absolute sensitivity; S_r, relative sensitivity.

imidazo[4,5-*f*][1,10]-phenanthroline have been reported, also Ln(HFAASi-SBA-15)$_3$phen, Ln = Eu^{3+}, Tb^{3+} (where HFAASi = modified hexafluoroacetylacetone; phen = 1,10-phenantroline), and phen-Ln-HTPP-SBA-15 as well as phen-Ln-PPIX-SBA-15, Ln = Nd^{3+}, Yb^{3+} (where HTPP = (meso-(tetra(*p*-hydroxyphenyl)porphyrin, PPIX = protoporphyrin IX) have been reported as unique examples of hybrid materials based on Ln^{3+} grafted onto organic-functionalized MS.[13–15]

In previous, recent work we functionalized a MS (as well as a PMO) material with dipyridyl-pyridazine (dppz) ligands and further covalently attached Er^{3+}, Yb^{3+} and Nd^{3+} complexes onto the dppz ligand.[16] Here, we further expand this work and prepare a Eu^{3+}/Tb^{3+} material (28.45% Eu:71.55% Tb, based on X-ray fluorescence (XRF)), which shows temperature-dependent luminescence properties and can be used as a ratiometric temperature sensor when observing the relative emission intensities of both the 544.0 nm Tb^{3+} peak and 611.0 nm Eu^{3+} peak.

In current literature, Ln^{3+} metal organic frameworks (LnMOFs) are among the most often reported Ln^{3+}-based luminescent thermometers materials as they demonstrate very promising temperature-dependent luminescence properties.[17,18] Many LnMOFs have already exhibited excellent thermometric behavior over a wide temperature range or specifically in the cryogenic region or in the physiological region. Among other materials, which have been explored as Ln^{3+}-based luminescent thermometers are Ln^{3+} doped inorganic phosphors, Ln^{3+} complexes, e.g. β-diketonate complexes and phosphonates, and very recently also Ln^{3+} polyoxometalates (LnPOMs).[19–24]

In this work we report an example of a mixed-lanthanide (Ln, Ln′) ratiometric thermometer material based on an organic-functionalized MS, where the MS was functionalized with dppz ligands to form the dppz-vSilica material, and in a later step post-functionalized with Eu^{3+}/Tb^{3+} ions (in the form of a chloride salt) to obtain the final hybrid material – dppz-vSilica@Eu,Tb.

2 | EXPERIMENTAL SECTION

2.1 | Synthesis

The dppz-vSilica@Ln (Ln = Eu^{3+}, Tb^{3+}) materials were obtained in a syntheses involving a few steps. In the first step, the substituted tetrazine was prepared in accordance to the procedure reported in the literature.[25] The vSilica and dppz-vSilica materials were prepared as described in our previous work.[16] Based on carbon–hydrogen–nitrogen (CHN) analysis the N% content in the dppz-vSilica material was determined to be 0.65%. Finally, dppz-vSilica@Ln materials were prepared by dissolving a certain amount of $LnCl_3{\cdot}6H_2O$ (Ln = Eu^{3+}, Tb^{3+}) in a certain amount of methanol and then adding the dppz-vSilica (solid) to the solution. The molar ratio of the $LnCl_3{\cdot}6H_2O$ to the dppz-vSilica was 4:1. The compounds were synthesized using a heating block set to 65°C (reaction carried out for 6 h). After cooling down the product was filtered and washed well with methanol. Afterwards it was dried using a vacuum oven set at 50°C. For the dppz-vSilica@Eu,Tb material a 1:1 ratio of the ions (Eu^{3+}:Tb^{3+}) was used in the synthesis. According to XRF analysis a dppz-vSilica@28.45%Eu, 71.55%Tb material was obtained in the synthesis.

2.2 | Characterization

Powder X-ray diffraction (PXRD) patterns were recorded on a Thermo Scientific ARL X'TRA diffractometer equipped with a Cu Kα (λ = 1.5405 Å) source, a goniometer and a Peltier cooled Si (Li) solid-state detector. Elemental analysis (CHN) was performed on a Thermo Flash 2000 elemental analyzer, V_2O_5 was used as the catalyst. To confirm the stability of the material thermogravimetric analysis (TGA) and differential thermal analysis (DTA) were performed on a Stanton Redcroft 1500 apparatus under air flow, in a temperature range from 20 to 800°C with a heating rate of 10°C min^{-1}. The Brunauer–Emmett–Teller (BET) surface areas were determined by nitrogen (N_2) physical adsorption–desorption isotherms obtained at 77 K on a Micromeritics Tristar II 3020 instrument. Prior to measurements, the samples were activated at 120°C for 3 h. By using the BET method the surface areas of the materials were calculated. The pore size distributions were obtained by analysis of the desorption branch of the isotherms using the Barrett–Joyner–Halenda (BJH) method. Energy dispersive XRF measurements were performed using an in-house developed μXRF instrument (at Ghent University Analytical Chemistry department).[26] The instrument has a monochromatic microfocus source (XOS, East Greenbush, NY, USA) and an SDD detector (e2v, Chelmsford, UK). The XRF spectra were analyzed using an AXIL software package.[27] To calculate the relative presence of the lanthanide elements (Eu, Tb) in the dppz-vSilica@Eu,Tb sample Monte–Carlo simulation aided quantification was used.[28] Photoluminescence measurements were performed using an Edinburgh Instruments FLSP920 UV-vis-NIR spectrometer setup. Solid powdered samples were put between quartz plates (Starna cuvettes for powdered samples, type 20/C/Q/0.2). A 450 W xenon lamp was used as the steady state excitation source. Decay times were recorded using a 60 W pulsed xenon lamp, operating at a frequency of 100 Hz. To detect the emission signals in the near UV to visible range a Hamamatsu R928P photomultiplier tube was used. Temperature-dependent luminescence measurements were performed using an ARS closed cycle cryostat operating in the temperature range between 4 and 360 K. All excitation spectra are recorded observing at the strongest f-f emission peak. All emission spectra in the manuscript have been corrected for detector response.

3 | RESULTS AND DISCUSSION

As described in our previous work the dppz-vSilica@Ln materials were obtained in a two-step procedure.[16] First, dppz-vSilica was obtained through the Diels–Alder reaction between the double bonds of the vSilica material and dppz ligand. In the next step the dppz-vSilica was functionalized with $EuCl_3$, $TbCl_3$ or a mixture of $EuCl_3$/$TbCl_3$ (Figure 1).

To characterize the materials (vSilica, dppz-vSilica and dppz-vSilica@Ln), PXRD, carbon-13 cross-polarization magic angle spinning nuclear magnetic resonance (^{13}C CP/MAS NMR), N_2 absorption–desorption, and XRF were performed. PXRDs of the vSilica, dppz-vSilica and dppz-vSilica@Ln (Ln = Eu^{3+}, Tb^{3+}, Eu^{3+}/Tb^{3+}) samples are presented in Figure 2. The PXRDs show that the dppz-vSilica and dppz-vSilica@Ln are very similar compared to the parent material –

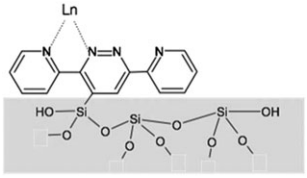

FIGURE 1 Schematic representation of bonding between dppz-vSilica and Ln^{3+} (Ln = Eu^{3+}, Tb^{3+})

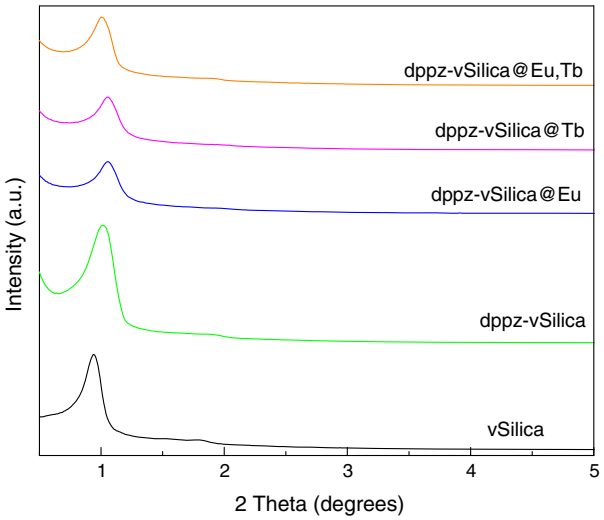

FIGURE 2 PXRD patterns of vSilica, dppz-vSilica, dppz-vSilica@Eu, dppz-vSilica@Tb, and dppz-vSilica@Eu,Tb

vSilica. This indicates that combining the vSilica with our organic ligand, as well as further grafting Ln^{3+} ions does not influence the structure of the parent material. In all of the diffractograms a strong reflection (100) at low 2θ, as well as two very weak second-order reflection peaks (110) and (200) can be observed. The PXRD confirm that the ordered hexagonal mesostructure (P_{6mm}) is preserved after the Diels–Alder reaction (to obtain dppz-vSilica) as well as after post-functionalization with Ln^{3+} salts.[2]

The N_2 adsorption–desorption isotherms of the vSilica and dppz-vSilica materials are shown in the Supporting Information Figure S1. Both the vSilica material, as well as the dppz-vSilica material, have type IV isotherms with H1-type hysteresis loops at relative pressures in the range 0.5–0.8. This is typical for mesoporous materials with uniform mesopores.[29,30] In Table 1 we have overviewed the BET surface area (S_{BET}), pore volume (V), pore diameter (D) and wall thickness (t) for the vSilica and dppz-vSilica materials. It can be concluded from these results that the surface area, pore volume, and pore size are smaller for the dppz-functionalized material. The S_{BET} decreased from 805 $m^2\ g^{-1}$ (for vSilica) to 176 $m^2\ g^{-1}$ after dppz-functionalization (dppz-vSilica). These results strongly suggest that the pores of the vSilica material have been combined with the Diels–Alder adduct. Similar observations have been reported for this type of reaction for other diens.[31]

TABLE 1 Structural parameters of the materials

Sample	d_{100} (nm)	S_{BET}($m^2\ g^{-1}$)	V ($cm^3\ g^{-1}$)	D (nm)[a]	t (nm)[b]
vSilica	9.4	805	0.92	6.4	4.4
dppz-vSilica	8.1	176	0.25	5.1	4.2

Note: d_{100}, (100) spacing; Brunauer–Emmett–Teller (BET) surface area; V, pore volume; D, pore diameter; t, wall thickness.

[a]Pore size by analysis of the desorption branch.

[b]Calculated from (a_0 – D_p), where $a_0 = 2d_{100}/\sqrt{3}$.

We have presented the solid-state ^{13}C CP/MAS NMR spectrum of the vSilica/dppz-vSilica materials in our previous work.[16] The luminescence properties of the dppz-vSilica@Ln materials were investigated. First, the room temperature luminescence properties of the dppz-vSilica@Eu and dppz-vSilica@Tb were studied. The emission spectra are presented in Figures 3 and 4, respectively.

The emission spectra were recorded when exciting the sample at 295.0 nm (into the dppz ligand band; see Figure S2) and they have been plotted with a rainbow under the curve to show the different color components. The dppz-vSilica@Eu sample showed the characteristic Eu^{3+} emission peaks: $^5D_0 \rightarrow {}^7F_0$ (576.0 nm), $^5D_0 \rightarrow {}^7F_1$ (586.0 nm), $^5D_0 \rightarrow {}^7F_2$ (611.0 nm), $^5D_0 \rightarrow {}^7F_3$ (650.0 nm), and $^5D_0 \rightarrow {}^7F_4$ (699.0 nm).[32] For the dppz-vSilica@Tb sample the characteristic Tb^{3+} emission peaks were detected: $^5D_4 \rightarrow {}^7F_6$ (487.0 nm), $^5D_4 \rightarrow {}^7F_5$ (544.0 nm), $^5D_4 \rightarrow {}^7F_4$ (582.0 nm), and $^5D_4 \rightarrow {}^7F_3$ (620.0 nm) (Figure 4).[33] A slight presence of the dppz ligand is noted in the lower wavelength range of the spectrum of both samples, this adds a blue color component to the materials.

The CIE color coordinates have been assessed for the dppz-vSilica@Eu and dppz-vSilica@Tb materials and have been marked on the CIE diagrams in Figures S3 and S4, respectively. Next, we

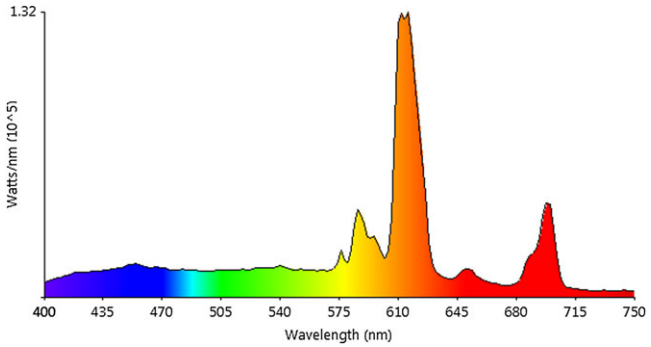

FIGURE 3 Room temperature emission spectrum of dppz-vSilica@Eu when excited at 295.0 nm. A rainbow has been plotted under the curve to show the different color components

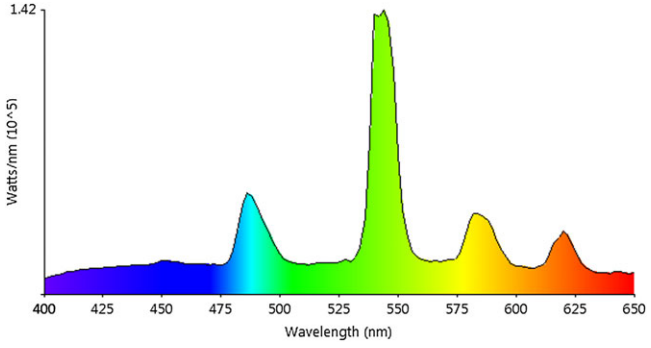

FIGURE 4 Room tempertaure emission spectrum of dppz-vSilica@Tb when excited at 295.0 nm. A rainbow has been plotted under the curve to show the different color components

investigated the decay times of the dppz-vSilica@Eu and dppz-vSilica@Tb materials. Their decay curves are presented in Figure S5 and S6, respectively. For both materials the curves can only be well fitted with a double-exponential function indicating that the materials have two luminescence lifetimes. The decay times of the dppz-vSilica@Eu material were calculated to be t_1 = 252 μs and t_2 = 18 μs (average decay time determined to be 65 μs; Figure S5). The decay times of the dppz-vSilica@Tb material were calculated to be t_1 = 179 μs and t_2 = 764 μs (average decay time determined to be 568 μs; Figure S6).

The luminescence properties of the dppz-vSilica@Eu,Tb material were investigated. At room temperature, when exciting the sample into the UV (see Figure S2), the $^5D_4 \rightarrow {}^7F_6$ (a) and $^5D_4 \rightarrow {}^7F_5$ (b) peaks of Tb^{3+} can be detected as well as the transition peaks of Eu^{3+}: $^5D_0 \rightarrow {}^7F_0$ (c), $^5D_0 \rightarrow {}^7F_1$ (d), $^5D_0 \rightarrow {}^7F_2$ (e), $^5D_0 \rightarrow {}^7F_3$ (f), and $^5D_0 \rightarrow {}^7F_4$ (g) (Figure 5). When exciting the sample at 322 nm (into the maximum of the broad ligand band) the same emission peaks are detected, but in a different relative ratio. When exciting the material at room temperature the Tb^{3+} peaks are more intensive, giving rise to a yellow-green emission color (see Figure S7). Exciting the dppz-vSilica@Eu,Tb sample in UV was chosen for its better performance as a ratiometric luminescence thermometer.

The decay times of the material have been recorded and are presented in Table 2. As can be seen from Table 2 in the dppz-vSilica@Eu,Tb material the (average) decay time observed at 611.0 nm (Eu^{3+}) is longer than for the dppz-vSilica@Eu material (Figure S8). However, the (average) decay time of the dppz-vSilica@Eu,Tb material (Figure S9) observed at 544.0 nm (Tb^{3+}) is shorter than that of the dppz-vSilica@Tb material. This would indicate that in the dppz-vSilica@Eu,Tb material energy is transferred from the ligand to Tb^{3+} and then to Eu^{3+}.

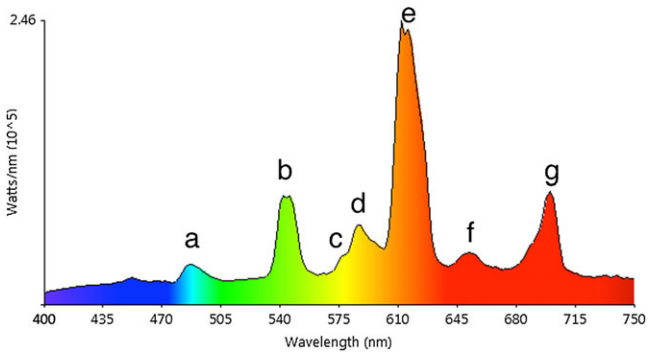

FIGURE 5 Room temperature emission spectrum of dppz-vSilica@Eu,Tb when excited at 295.0 nm. A rainbow has been plotted under the curve to show the different color components. The assignment of letters a–g to appropriate transitions has been given in the text

TABLE 2 Luminescence decay times of Eu, Tb and Eu,Tb mesoporous materials

Sample	τ_1 (μs)/%	τ_2 (μs)/%	τ_{av} (μs)
dppz-vSilica@Eu	18/98	292/2	65
dppz-vSilica@Tb	179/68	764/32	568
dppz-vSilica@Eu,Tb (observed Eu^{3+})	182/74	390/26	270
dppz-vSilica@Eu,Tb (observed Tb^{3+})	118/74	490/26	340

Note: average decay time calculated according to equation S1 (see Supporting Information).

Next, The temperature-dependent luminescence properties of the dppz-vSilica@Eu,Tb material were studied so that its potential use as a thermometer could be evaluated. Thermometers based on the intensity ratio of two transitions (e.g. Eu^{3+} and Tb^{3+}), so called ratiometric thermometers, overcome certain drawbacks such as fluctuations of the excitation source.[34] Here, we study the well-known Eu^{3+}-to-Tb^{3+} emission ratio, but in a novel type of material – namely in an organic-functionalized MS.

To study dual-center thermometers, such as in this case, the commonly used conversion of intensity into temperature is made via the thermometric parameter Δ (equations 1 and 2):

$$\Delta = \frac{I_1}{I_2} \tag{1}$$

$$\Delta = \frac{\Delta_0}{1 + \alpha \exp\left(-\frac{\Delta E}{k_B T}\right)} \tag{2}$$

where I_1 and I_2 are the integrated intensities of the two transitions, Δ_0 is the thermometric parameter at T = 0 K, $\alpha = W_0/W_R$ the ratio between the non-radiative (W_0 at T = 0 K) and radiative (W_R) rates, and ΔE is the activation energy for the non-radiative channel.[35] The absolute (S_a) and relative (S_r) temperature sensitivity can be determined using the following equations (equations 3 and 4)[36,37]:

$$S_a = \left|\frac{\partial \Delta}{\partial T}\right| \tag{3}$$

$$S_r = 100\% \times \left|\frac{1}{\Delta}\frac{\partial \Delta}{\partial T}\right| \tag{4}$$

The emission map of the dppz-vSilica@Eu,Tb material measured over a temperature range of 10 to 360 K (step size of 50 K) is presented in Figure 6.

The emission spectra were not measured above 360 K as the Tb^{3+} peaks were already very weak in intensity at this temperature range. In the 10–360 K temperature range we see a general trend that with temperature increase the emission intensity of Tb^{3+} decreases. Above around 310 K we can observe that there is a more efficient energy transfer between Tb^{3+}-Eu^{3+} as the Eu^{3+} peaks significantly increase in intensity. Similar behavior in Tb^{3+}-Eu^{3+} compounds has previously been reported in the literature.[38,39]

In the excitation spectrum we only observe a change in intensity (and slight change of shape) of the broad ligand band with temperature change (Figure S10). The emission color of the material was also observed with temperature change. As can be seen from Figure 7, at 10 K the emission color of the material is yellow, with temperature increasing towards 310 to 360 K it changes to orange and then red.

To evaluate the use of this material as a ratiometric temperature sensor the I_{544}/I_{611} ratio of the integrated areas calculated have been plotted in Figure 8 (calculated integrated areas: 531–564 nm for Tb^{3+} and 602–638 nm for Eu^{3+}). The data points were well fitted using equation 2, yielding Δ_0 = 1.749, α = 602.18, and ΔE = 1115 cm^{-1}

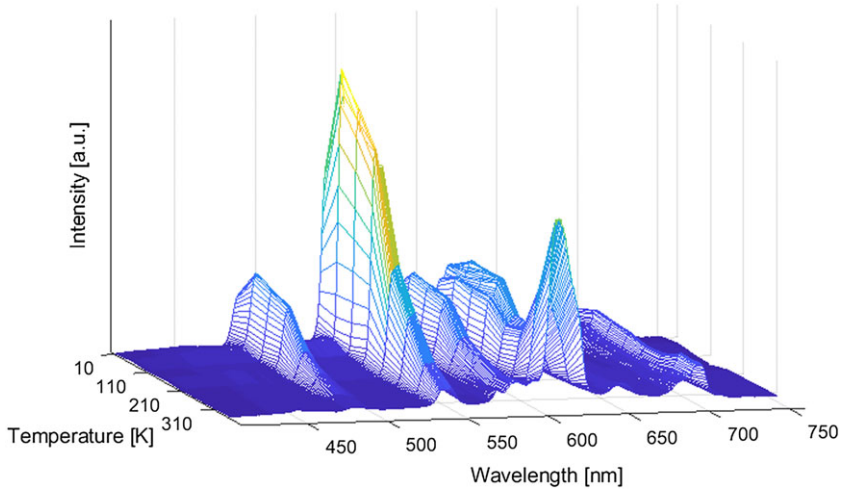

FIGURE 6 Emission map of dppz-vSilica@Eu,Tb measured at varying temperatures (10–360 K; step size 50 K)

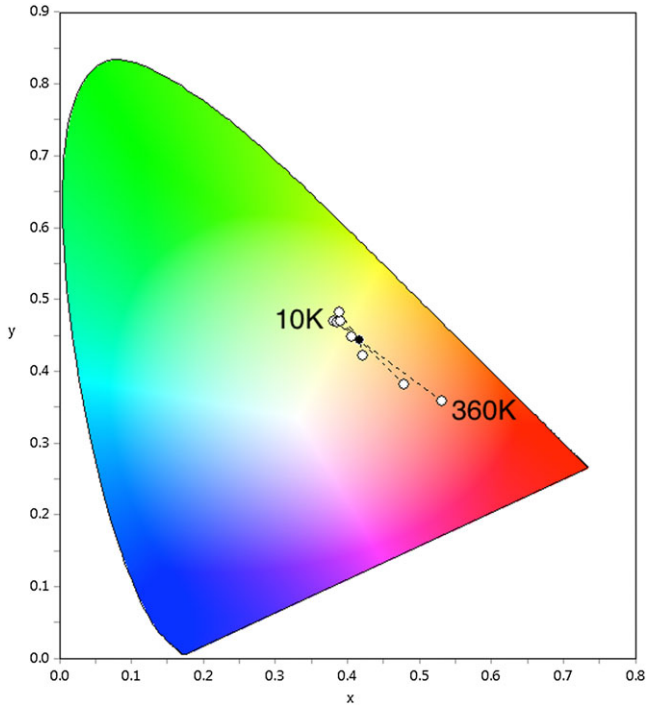

FIGURE 7 CIE color diagram showing the *x* and *y* color coordinates of the dppz-vSilica@Eu,Tb material at different temperatures (see Supporting Information Table S1 for exact *x* and *y* coordinates at different temperatures)

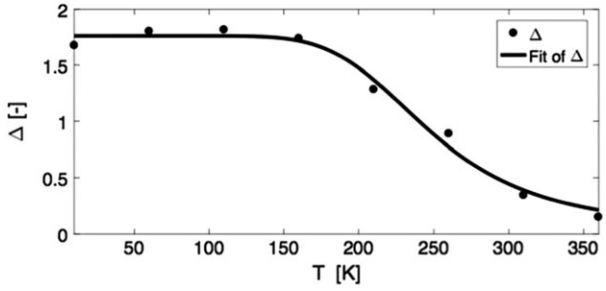

FIGURE 8 Plot presenting the evolution with temperature of the thermometric parameter for the dppz-vSilca@Eu,Tb material. The points depict the experimental parameter and the solid line represents the calibration curve obtained by the best fit of the experimental points

(R^2 = 0.988). In Figure 9 we have presented the absolute sensitivity S_a values and the relative sensitivity S_r values, calculated for the different temperatures. The maximum value of the S_a and S_r are 0.011 K^{-1} (210 K) and 1.32 $\%K^{-1}$ (260 K), respectively. In Table 3 we have overviewed some recently reported thermometer materials (S_r values) based on Eu-Tb observed in a similar temperature range as our dppz-vSilica@Eu,Tb material to compare our result with those found in the literature. Although other lanthanides and co-doped lanthanide (e.g. Er^{3+}/Yb^{3+})[50,51] materials such as MOFs[52] are often reported, our dppz-vSilica@Eu,Tb material shows promising performance as a ratiometric luminescence thermometer.[53]

In a last step we performed TG-DTA on the thermometric sample to confirm its stability in the temperature region it was tested (up to 360 K) (see Figure S11).

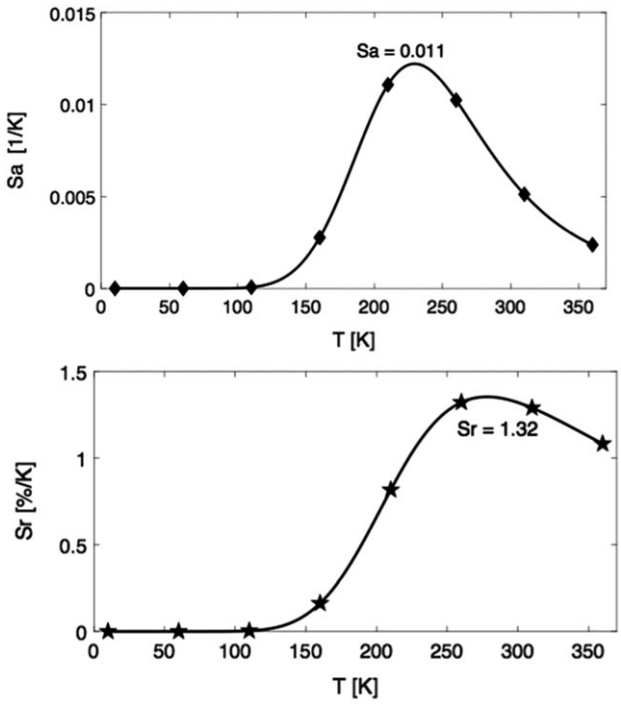

FIGURE 9 Top: plot presenting S_a values at different temperatures (10–360 K) for dppz-vSilica@Eu,Tb. Bottom: plot presenting S_r values in the same temperature range. The solid lines are a guide for the eyes

TABLE 3 Overview of the relative sensitivity S_r (highest value) of some recently reported ratiometric thermometer materials (materials which have been tested in a similar temperature range to our material are presented)

Material	Temperature range (K)	Maximum S_r ($\%K^{-1}$)	Temperature- dependent algorithm	Reference
$Tb_{0.957}Eu_{0.043}$cpda	40–300	1.77 (250 K)	I_{Tb}/I_{Eu}	[40]
$Eu_{0.02}Gd_{0.98}$(DSB)	20–300	4.75 (20 K)	$I_{Triplet}/I_{Eu}$	[41]
$\{Tb_{0.3}Eu_{0.7}$ (D-cam)$(Himdc)_2\cdot(H_2O)_2\}_3$	100–450	0.11 (450 K)	I_{Tb}/I_{Eu}	[18,42]
$[(Tb_{0.914}Eu_{0.086})_2(pda)_3(H_2O)]\cdot 2H_2O$	10–325	5.96 (25 K)	I_{Tb}/I_{Eu}	[43]
$Tb_{0.005}Eu_{0.995}$@UiO-67-bpydc	100–300	3.01 (180 K)	I_{Tb}/I_{Eu}	[44]
$Tb_{0.9}Eu_{0.1}$L	40–300	0.11 (300 K)	I_{Tb}/I_{Eu}	[45]
$Tb_{0.8}Eu_{0.2}$L	40–300	0.15 (300 K)	I_{Tb}/I_{Eu}	[45]
$Tb_{0.7}Eu_{0.3}$L	40–300	0.17 (300 K)	I_{Tb}/I_{Eu}	[45]
$Tb_{0.95}Eu_{0.05}$HY	4–300	31 (4 K)	I_{Eu}/I_{Tb}	[46]
$Tb_{0.95}Eu_{0.05}$(btb)	10–320	2.85 (14 K)	I_{Tb}/I_{Eu}	[47]
$Eu_{0.25}Tb_{0.75}(btfa)_3$ (MeOH)(bpeta)]	10–330	4.90 (150 K)	I_{Tb}^2-I_{Eu}^2	[48]
$NaGdF_4$:Yb/Tm@Tb/Eu	125–300	0.49 (300 K)	I_{Tb}/I_{Eu}	[49]
$Na[(Gd_{0.8}Eu_{0.1}Tb_{0.1})\ SiO_4]$	12–450	2.00 (20 K)	I_{Tb}/I_{Eu}	[35]
$Eu_{0.102}Tb_{0.898}(notpH_4)(NO_3)(H_2O)]\cdot 8H_2O$	18–300	3.90 (38 K)	I_{Tb}/I_{Eu}	[23]
dppz-vSilica@Eu,Tb	10–360	**1.32 (260 K)**	I_{Tb}/I_{Eu}	This work

4 | CONCLUSION

In this work we show that Eu^{3+}/Tb^{3+} grafted organic-functionalized MS can be employed successfully as a ratiometric temperature sensor. The material shows monotonic behavior in the temperature range of 160 to 360 K. Above 360 K the peaks of Tb^{3+} are barely distinguishable from the background noise, and therefore it is not further considered as a sensor at higher temperatures. The emission color of the sample changes gradually from yellow (10 K) to red (360 K). An absolute sensitivity S_a of 0.011 K^{-1} (210 K) and relative sensitivity S_r of 1.32 $\%K^{-1}$ (260 K) were obtained showing good sensing capability of the material. Here, we have presented a new class of materials, namely Ln-Ln′ (Eu^{3+}-Tb^{3+}) decorated organic-functionalized MS as a potential ratiometric thermometer.

ACKNOWLEDGMENTS

AMK thanks Ghent University's Special Research Fund (BOF) for a Postdoctoral Mandate (project BOF15/PDO/091). DE and FJRS acknowledges funding of this research by the Spanish Ministry of Economy and Competitiveness (Project MAT2013-44463-R), Andalusian Regional Government (FQM-346 group), and Feder Funds.

ORCID

Anna M. Kaczmarek http://orcid.org/0000-0001-5254-8762
Dolores Esquivel http://orcid.org/0000-0002-4323-8698
Pascal Van Der Voort http://orcid.org/0000-0002-1248-479X
Francisco J. Romero-Salguero http://orcid.org/0000-0001-7494-9196
Rik Van Deun http://orcid.org/0000-0001-7091-6864

REFERENCES

[1] X. Guo, H. Guo, L. Fu, H. Zhang, R. Deng, L. Sun, J. Feng, S. Dang, *Microporous Mesoporous Mat.* **2009**, *119*, 252.

[2] D. Esquivel, A. M. Kaczmarek, C. Jimenez-Sanchidrian, R. Van Deun, F. J. Romero-Salguero, P. Van Der Voort, *J. Mater. Chem. C* **2015**, *3*, 2909.

[3] L. N. Sun, H. J. Zhang, C. Y. Peng, J. B. Yu, Q. G. Meng, L. S. Fu, F. Y. Liu, X. M. Guo, *J. Phys. Chem. B* **2006**, *110*, 7249.

[4] L. N. Sun, H. J. Zhang, J. B. Yu, S. Y. Yu, C. Y. Peng, S. Dang, X. M. Guo, J. Feng, *Langmuir* **2008**, *24*, 5500.

[5] L. Sun, W. Mai, S. Dang, Y. Qui, W. Deng, L. Shi, W. Yan, H. Zhang, *J. Mater. Chem.* **2012**, *22*, 5121.

[6] B. Yan, B. Zhou, *J. Photochem. Photobiol. A Chem.* **2008**, *195*, 314.

[7] H. Yang, N. Coombs, G. A. Ozin, *Nature* **1997**, *386*, 692.

[8] Z. A. Alothman, *Materials* **2012**, *5*, 2874.

[9] J.-C. G. Bunzli, C. Piguet, *Chem. Soc. Rev.* **2005**, *34*, 1048.

[10] M. H. Werts, *Sci. Prog.* **2005**, *88*, 101.

[11] K. Binnemans, *Chem. Rev.* **2009**, *109*, 4283.

[12] L. D. Carlos, R. A. S. Ferreira, V. de Zea Bermudez, S. J. L. Ribeiro, *Adv. Mater.* **2009**, *21*, 509.

[13] Y. Liu, L. Sun, J. Liu, Y.-X. Peng, X. Ge, L. Shi, W. Huang, *Dalton Trans.* **2015**, *44*, 237.

[14] Y.-J. Li, X. Yu, X. Wang, M. Yang, *J. Mater. Res.* **2014**, *29*, 675.

[15] B. Yan, Y.-Y. Li, X.-F. Qiao, *Microporous Mesoporous Mat.* **2012**, *158*, 129.

[16] A. M. Kaczmarek, D. Esquivel, J. Ouwehand, P. Van Der Voort, F. J. Romero-Salguero, R. Van Deun, *Dalton Trans.* **2017**, *46*, 7878.

[17] Y. Cui, F. Zhu, B. Chen, G. Qian, *Chem. Commun.* **2015**, *51*, 7420.

[18] J. Rocha, C. D. S. Brites, L. D. Carlos, *Chem. - Eur. J.* **2016**, *22*, 14782.

[19] R. G. Geitenbeek, P. T. Prins, W. Albrecht, A. van Blaaderen, B. M. Weckhuysen, A. Meijerink, *J. Phys. Chem. C* **2017**, *121*, 3503.

[20] D. Wawrzynczyk, A. Bednarkiewicz, M. Nyk, W. Strek, M. Samoc, *Nanoscale* **2012**, *4*, 6959.

[21] C. D. S. Brites, P. P. Lima, L. D. Carlos, *J. Lumin.* **2016**, *169*, 497.

[22] P. P. Lima, F. A. A. Paz, C. D. S. Brites, W. G. Quirino, C. Legnani, M. Costa, E. Silva, R. A. S. Ferreira, S. A. Junior, O. L. Malta, M. Cremona, L. D. Carlos, *Org. Electron.* **2014**, *15*, 798.

[23] M. Ren, C. D. S. Brites, S.-S. Bao, R. A. S. Ferreira, L.-M. Zheng, L. D. Carlos, *J. Mater. Chem. C* **2015**, *3*, 8480.

[24] A. M. Kaczmarek, J. Liu, B. Laforce, L. Vincze, K. Van Hecke, R. Van Deun, *Dalton Trans.* **2017**, *46*, 5781.

[25] M. S. Robillard, H. M. Janssen, W. ten Hoeve, R. M. Versreegen, US pat. 9421274 B2, **2016**

[26] J. Garrevoet, B. Vekemans, S. Bauters, A. Demey, L. Vincze, *Anal. Chem.* **2015**, *87*, 6544.

[27] B. Vekemans, K. Janssens, L. Vincze, F. Adams, P. Vanespen, *X-Ray Spectrom.* **1994**, *23*, 278.

[28] T. Schoonjans, V. A. Sole, L. Vincze, M. Sanchez del Rio, K. Appel, C. Ferrero, *Spectrochim. Acta, Part B* **2013**, *82*, 36.

[29] C. G. Sonwane, S. K. Bhatia, *J. Phys. Chem. B* **2000**, *104*, 9099.

[30] K. Sing, *Coll. Surf. A: Physiochem. Eng. Aspects* **2001**, *187-188*, 3.

[31] D. Esquivel, E. De Canck, C. Jimenez-Sanchidrian, P. Van Der Voort, F. J. Romero-Salguero, *J. Mater. Chem.* **2011**, *21*, 10990.

[32] K. Binnemans, *Coord. Chem. Rev.* **2015**, *295*, 1.

[33] A. M. Kaczmarek, D. Ndagsi, I. Van Driessche, K. Van Hecke, R. Van Deun, *Dalton Trans.* **2015**, *44*, 10237.

[34] C. D. S. Brites, P. P. Lima, N. J. O. Silva, A. Millan, V. S. Amaral, F. Palacio, L. D. Carlos, *New J. Chem.* **2011**, *35*, 1177.

[35] D. Ananias, F. A. A. Paz, D. S. Yufit, L. D. Carlos, *J. Am. Soc.* **2015**, *137*, 3051.

[36] C. D. S. Brites, P. P. Lima, N. J. O. Silva, A. Millan, V. S. Amaral, F. Palacio, L. D. Carlos, *Nanoscale* **2012**, *4*, 4799.

[37] L. D. Carlos, F. Palacio, *Thermometry at the Nanoscale: Techniques and Selected Applications*, Royal Society of Chemistry, Oxfordshire **2016**.

[38] Y. Cui, H. Xu, Y. Yue, Z. Guo, J. Yu, Z. Chen, J. Gao, Y. Yang, G. Qian, B. Chen, *J. Am. Chem. Soc.* **2012**, *134*, 3979.

[39] A. M. Kaczmarek, Y.-Y. Liu, C. Wang, B. Laforce, L. Vincze, P. Van Der Voort, K. Van Hecke, R. Van Deun, *Adv. Funct. Mater.* **2017**, 1700258.

[40] Y. J. Cui, W. F. Zou, R. J. Song, J. C. Yu, W. Q. Zhang, Y. Yang, G. D. Qian, *Chem. Commun.* **2014**, *50*, 719.

[41] R. F. D'Vries, S. Alvarez-Garcia, N. Snejko, L. E. Bausa, E. Gutierrez-Puebla, A. de Andres, M. A. Monge, *J. Mater. Chem. C* **2013**, *1*, 6316.

[42] Y. H. Han, C. B. Tian, Q. H. Li, S. W. Du, *J. Mater. Chem. C* **2014**, *2*, 8065.

[43] Z. P. Wang, D. Ananias, A. Carne-Sanchez, C. D. S. Brites, I. Imaz, D. Maspoch, J. Rocha, L. D. Carlos, *Adv. Funct. Mater.* **2015**, *25*, 2824.

[44] Y. Zhou, B. Yan, *J. Mater. Chem. C* **2015**, *3*, 9353.

[45] S. N. Zhao, L. J. Li, X. Z. Song, M. Zhu, Z. M. Hao, X. Meng, L. L. Wu, J. Feng, S. Y. Song, C. Wang, H. J. Zhang, *Adv. Funct. Mater.* **2015**, *25*, 1463.

[46] X. Liu, S. Akerboom, M. se Jong, I. Mutikainen, S. Tanase, A. Meijerink, E. Bouwman, *Inorg. Chem.* **2015**, *54*, 11323.

[47] D. Ananias, C. D. Brites, L. D. Carlos, J. Rocha, *Eur. J. Inorg. Chem.* **2016**, 1967.

[48] C. D. S. Brites, P. P. Lima, N. J. O. Silva, A. Millan, V. S. Amaral, F. Palacio, L. D. Carlos, *Adv. Mater.* **2010**, *22*, 4499.

[49] S. H. Zheng, W. B. Chen, D. Z. Tan, J. J. Zhou, Q. B. Guo, W. Jiang, C. Xu, X. F. Liu, J. R. Qiu, *Nanoscale* **2014**, *6*, 5675.

[50] L. Mukhopadhyay, V. K. Rai, R. Bokolia, K. Sreenivas, *J. Lumin.* **2017**, *187*, 368.

[51] R. Dey, A. Pandey, V. K. Rai, *Sens. Actuator B-Chem* **2014**, *190*, 512.

[52] A. Cadiau, C. D. S. Brites, P. M. F. J. Costa, R. A. S. Ferreira, J. Rocha, L. D. Carlos, *ACS Nano* **2013**, *7*, 7213.

[53] V. K. Rai, *Appl. Phys. B: Lasers Opt.* **2007**, *88*, 297.

SUPPORTING INFORMATION

Additional Supporting Information may be found online in the supporting information tab for this article.

How to cite this article: Kaczmarek AM, Esquivel D, Laforce B, et al. Luminescent thermometer based on Eu^{3+}/Tb^{3+}-organic-functionalized mesoporous silica. *Luminescence*. 2018;33:567–573. https://doi.org/10.1002/bio.3447